Langmuir Article

pubs.acs.org/Langmuir

L-Cysteine-Assisted Growth of Core−Satellite ZnS−Au Nanoassemblies with High Photocatalytic Efficiency

Wei-Ta Chen and Yung-Jung Hsu*

Department of Materials Science and Engineering, National Chiao Tung University, Hsinchu, Taiwan 30010, Republic of China

Received October 12, 2009

Core−satellite ZnS−Au nanoassemblies, in which each of the ZnS nanospheres was surrounded by a few Au nanoparticles, have been successfully prepared with a facile L-cysteine-assisted hydrothermal approach. The density of Au nanoparticles encircling each ZnS nanosphere can be readily controlled through suitably modulating the concentration of Au added. Because of the difference in band structures between ZnS and Au, a pronounced photoinduced charge separation was observed for the as-synthesized ZnS−Au nanoassemblies. As compared to the relevant commercial products like Au-loaded P-25 TiO_2 and ZnS powders, ZnS−Au nanoassemblies exhibited superior photocatalytic performance, demonstrating their potential as an efficient photocatalyst in relevant redox reactions. Furthermore, the recycling test revealed that core−satellite nanoassemblies of ZnS−Au could be promisingly utilized in the long-term course of photocatalysis. The present study provides a new paradigm for designing the highly efficient semiconductor/metal hybrid photocatalysts that can effectively produce chemical energy from light.

Introduction

Photocatalysis for water splitting and pollutant degradation using semiconductors is of great interest because of its capability of converting light energy into chemical energy.[1] Various semiconductor photocatalysts have thus been developed to carry out chemical reactions under light illumination. Among them, ZnS is one of the most popular photocatalysts that have been extensively studied. The rapid generation of charge carriers upon light irradiation and the relatively negative reduction potential of excited electrons offer ZnS good photocatalytic activities.[2] Until now, many structural forms of ZnS including nanoparticles,[2,3] nanospheres,[4] porous nanoparticles,[5] hollow spheres,[6] nanowalls,[7] and nanorods[8] have been proven effective in relevant photocatalytic processes.

Like TiO_2, ZnS possesses a wide bandgap energy (E_g = 3.7 eV) and can absorb light only in the ultraviolet range, which may limit its practical development in photocatalysis. Furthermore, the photocatalytic efficiency of ZnS is commonly depressed by the fast recombination of photoexcited charge carriers. Hence, an effort to either modulate the band structure of ZnS to allow photocatalysis under visible light or suppress the direct recombination of charge carriers to enhance the photocatalytic performance of ZnS is being pursued. For example, through the introduction of suitable dopants to create an additional donor level in the energy gap, ZnS could be capable of light absorption in the visible range.[9,10] Besides, by alloying with other narrow-bandgap semiconductors, one may obtain ZnS-based solid solution whose bandgap energy can be readily tuned.[11,12] On the other hand, to retard the radiative recombination of charge carriers in ZnS, an electron trapper such as TiO_2,[13] carbon nanotube,[14] and metal[15] was often introduced and put in contact with ZnS. It is worth noting that semiconductors may exhibit superior photocatalytic activities through simply combining with metals. This is due to the presence of semiconductor/metal interface that can induce effective charge separation to favor the subsequent photocatalysis.[16] As a result, miscellaneous kinds of semiconductor/metal hybrid systems such as core−shell metal−semiconductor nanocrystals,[15,17] metal-decorated

*Corresponding author. E-mail: yhsu@cc.nctu.edu.tw.

(1) Linsebigler, A. L.; Lu, G.; Yates, J. T. *Chem. Rev.* **1995**, *95*, 735.
(2) (a) Yanagida, S.; Ishimaru, Y.; Miyake, Y.; Shiragami, T.; Pac, C.; Hashimoto, K.; Sakata, T. *J. Phys. Chem.* **1989**, *93*, 2516. (b) Yanagida, S.; Yoshiya, M.; Shiragami, T.; Pac, C.; Mori, H.; Fujita, H. *J. Phys. Chem.* **1990**, *94*, 3104. (c) Kanemoto, M.; Shiragami, T.; Pac, C.; Yanagida, S. *J. Phys. Chem.* **1992**, *96*, 3521.
(3) (a) Fujiwara, H.; Hosokawa, H.; Murakoshi, K.; Wada, Y.; Yanagida, S. *Langmuir* **1998**, *14*, 5154. (b) Ni, Y.; Cao, X.; Hu, G.; Yang, Z.; Wei, X.; Chen, Y.; Xu, J. *Cryst. Growth Des.* **2007**, *7*, 280.
(4) (a) Zhao, Q.; Xie, Y.; Zhang, Z.; Bai, X. *Cryst. Growth Des.* **2007**, *7*, 153. (b) Li, Y.; He, X.; Cao, M. *Mater. Res. Bull.* **2008**, *43*, 3100.
(5) (a) Hu, J.-S.; Ren, L.-L.; Guo, Y.-G.; Liang, H.-P.; Cao, A.-M.; Wan, L.-J.; Bai, C.-L. *Angew. Chem., Int. Ed.* **2005**, *44*, 1269. (b) Yang, J.; Peng, J.; Zou, R.; Peng, F.; Wang, H.; Yu, H.; Lee, J.-Y. *Nanotechnology* **2008**, *19*, 255603.
(6) Yu, X.; Yu, J.; Cheng, B.; Huang, B. *Chem.—Eur. J.* **2009**, *15*, 6731.
(7) Lu, M.-Y.; Lu, M.-P.; Chung, Y.-A.; Chen, M.-J.; Wang, Z.-L.; Chen, L.-J. *J. Phys. Chem. C* **2009**, *113*, 12878.
(8) (a) Xiong, S.; Xi, B.; Wang, C.; Xu, D.; Feng, X.; Zhu, Z.; Qian, Y. *Adv. Funct. Mater.* **2007**, *17*, 2728. (b) Xi, G.; Wang, C.; Wang, X.; Zhang, Q.; Xiao, H. *J. Phys. Chem. C* **2008**, *112*, 1946.
(9) (a) Kudo, A.; Sekizawa, M. *Catal. Lett.* **1999**, *58*, 241. (b) Kudo, A.; Sekizawa, M. *Chem. Commun.* **2000**, 1371. (c) Tsuji, I.; Kudo, A. *J. Photochem. Photobiol. A* **2003**, *156*, 249.
(10) (a) Arai, T.; Senda, S.; Sato, Y.; Takahashi, H.; Shinoda, K.; Jeyadevan, B.; Tohji, K. *Chem. Mater.* **2008**, *20*, 199. (b) Muruganandham, M.; Kusumoto, Y. *J. Phys. Chem. C* **2009**, *113*, 16144.
(11) (a) Tsuji, I.; Kato, H.; Kobayashi, H.; Kudo, A. *J. Am. Chem. Soc.* **2004**, *126*, 13406. (b) Tsuji, I.; Kato, H.; Kudo, A. *Angew. Chem., Int. Ed.* **2005**, *44*, 3565. (c) Tsuji, I.; Kato, H.; Kobayashi, H.; Kudo, A. *J. Phys. Chem. B* **2005**, *109*, 7323. (d) Tsuji, I.; Kato, H.; Kudo, A. *Chem. Mater.* **2006**, *18*, 1969. (e) Li, Y.; Chen, G.; Zhou, C.; Sun, J. *Chem. Commun.* **2009**, 2020.
(12) (a) Liu, G.; Zhao, L.; Ma, L.; Guo, L. *Catal. Commun.* **2008**, *9*, 126. (b) Zhang, X.; Jing, D.; Liu, M.; Guo, L. *Catal. Commun.* **2008**, *9*, 1720. (c) Zhang, W.; Zhong, Z.; Wang, Y.; Xu, R. *J. Phys. Chem. C* **2008**, *112*, 17635.
(13) (a) Leez, M.-K.; Shih, T.-H. *J. Electrochem. Soc.* **2007**, *154*, 49.
(14) (a) Feng, S.-A.; Zhao, J.-H.; Zhu, Z.-P. *New Carbon Mater.* **2008**, *23*, 228. (b) Wu, H.; Wang, Q.; Yao, Y.; Qian, C.; Zhang, X.; Wei, X. *J. Phys. Chem. C* **2008**, *112*, 16779.
(15) Sun, Z.; Yang, Z.; Zhou, J.; Yeung, M. H.; Ni, W.; Wu, H.; Wang, J. *Angew. Chem., Int. Ed.* **2009**, *48*, 2881.
(16) (a) Subramanian, V.; Wolf, E. E.; Kamat, P. V. *J. Phys. Chem. B* **2003**, *107*, 7479. (b) Jakob, M.; Levanon, H.; Kamat, P. V. *Nano Lett.* **2003**, *3*, 353. (c) Subramanian, V.; Wolf, E. E.; Kamat, P. V. *J. Am. Chem. Soc.* **2004**, *126*, 4943. (d) Costi, R.; Cohen, G.; Salant, A.; Rabani, E.; Banin, U. *Nano Lett.* **2009**, *9*, 2031.
(17) (a) Kamat, P. V.; Shanghavi, B. *J. Phys. Chem. B* **1997**, *101*, 7675. (b) Hirakawa, T.; Kamat, P. V. *J. Am. Chem. Soc.* **2005**, *127*, 3928. (c) Sakai, H.; Kanda, T.; Shibata, H.; Ohkubo, T.; Abe, M. *J. Am. Chem. Soc.* **2006**, *128*, 4944. (d) Shi, W.; Zeng, H.; Sahoo, Y.; Ohulchanskyy, T. Y.; Ding, Y.; Wang, Z. L.; Swihart, M.; Prasad, P. N. *Nano Lett.* **2006**, *6*, 875. (e) Lee, J.-S.; Shevchenko, E. V.; Talapin, D. V. *J. Am. Chem. Soc.* **2008**, *130*, 9673. (f) Wu, X.-F.; Song, H.-Y.; Yoon, J.-M.; Yu, Y.-T.; Chen, Y.-F. *Langmuir* **2009**, *25*, 6438.

semiconductor nanorods,[18] and metal-deposited semiconductor nanoparticles[19] have been proposed to further the development of photocatalysts. There are however very few studies in the literature concerning the fabrication of ZnS/metal hybrid materials, and their performance in photocatalysis is rarely reported. Therefore, creation of a synthetic route to fabricate ZnS/metal hybrid photocatalysts is still a challenging task at present.

In this work, we present a prototype ZnS/metal hybrid system by synthesizing core−satellite ZnS−Au nanoassemblies, in which each of the ZnS nanospheres was surrounded by a few Au nanoparticles, with a facile hydrothermal method. We analyzed the details of hydrothermal growth, discussed the optical properties of the nanoassembly products, and investigated for the first time the photocatalytic performance of ZnS/Au hybrid system. The formation of ZnS−Au nanoassemblies involved the binding of Au nanoparticles toward L-cysteine−Zn^{2+} complexes (Cys/Zn), followed by the hydrothermal decomposition of Cys/Zn and the subsequent growth of ZnS nanospheres that were surrounded by Au nanoparticles. By suitably modulating the concentration of Au added, a controllable density of Au nanoparticles that encircled each ZnS nanosphere can be achieved. Because of the difference in band structures between ZnS and Au, a pronounced photoinduced charge separation was observed for the as-synthesized ZnS−Au nanoasssembles. For ZnS−Au, the satellite Au can serve as an effective electron trapper for the core ZnS due to its lower Fermi energetic level (+0.5 V vs NHE)[17a] than the conduction band of ZnS (−1.85 V vs NHE).[20] Consequently, the photoexcited free electrons in ZnS would preferentially transfer to Au, leaving positively charged holes in ZnS to achieve charge carrier separation. These separated charge carriers are highly reactive in redox reactions, giving rise to a promising performance in the course of photocatalysis. Scheme 1 illustrates the hydrothermal growth of ZnS−Au nanoassemblies and depicts the interfacial charge transfer processes that occurred in ZnS−Au. We evaluated the photocatalytic performance of ZnS−Au nanoassemblies through the photodegradation of an organic dye, thionine (TH), under ultraviolet (UV) illumination. As compared to the relevant commercial products like Au-loaded P-25 TiO_2 and ZnS powders, the as-synthesized ZnS−Au nanoassemblies exhibited superior photocatalytic performance toward TH photodegradation, attributable to the effective charge separation that took place at the interface of ZnS/Au. Moreover, no appreciable decay of photocatalytic activity was found for ZnS−Au nanoassemblies after repeated uses and recycled, demonstrating their promising potential in the long-term course of photocatalysis.

Experimental Section

Chemicals. All chemicals were of analytic grade and used without further purification.

Preparation of Au Colloids. Au colloids were synthesized by the conventional citrate reduction method.[21] In a typical synthesis, an aqueous solution of tetrachloroauric acid ($HAuCl_4$, 100 mL, 0.25 mM) was heated to boiling, followed by the rapid addition of trisodium citrate solution ($Na_3C_6H_5O_7$, 200 μL, 0.5 M). The resulting solution was kept boiling for about 10 min, producing a stable, deep-red dispersion of Au nanoparticles with an average diameter of about 15 nm. The well-dispersed Au colloids were then cooled to room temperature for later use.

Scheme 1. Schematic Illustration of the Synthesis of Core−Satellite ZnS−Au Nanoassemblies and the Interfacial Charge Transfer Processes That Occurred in ZnS−Au

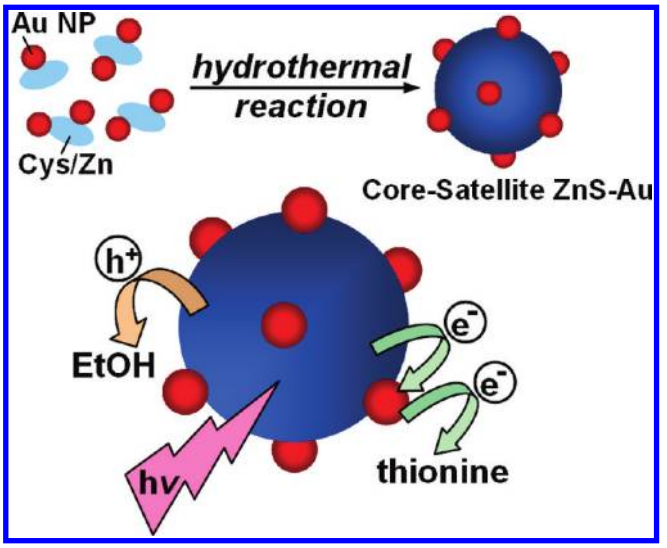

Preparation of Core−Satellite ZnS−Au Nanoassemblies. An aqueous solution of L-cysteine ($C_3H_7NO_2S$, denoted as Cys, 50 mM) was mixed with zinc nitrate ($Zn(NO_3)_2$) in a 1:0.5 molar ratio of Cys to Zn^{2+}. The resulting mixture was stirred for 30 min to form the stable complexes of L-cysteine−Zn^{2+} (denoted as Cys/Zn). The freshly prepared Cys/Zn (4 mL, 50 mM) was then added to a given amount of Au colloids (9 mL, 45 μM) under vigorous stirring for 30 min, leading to a complete coupling between amine groups of Cys and Au surfaces. Subsequently, the Au-coupled Cys/Zn (denoted as (Cys/Zn)−Au) were diluted to a total volume of 50 mL with deionized water and transferred into a Teflon-lined stainless-steel autoclave with a capacity of 100 mL. After being sealed, the autoclave was heated and maintained at 130 °C for 6 h and then cooled to room temperature naturally. The product (ZnS−Au nanoassemblies) was collected by centrifugation at 8500 rpm for 10 min and washed with distilled water and ethanol to remove remaining ions and impurities.

Density Control for Satellite Au. Au colloids of four various concentrations (45, 90, 180, and 225 μM) were employed in this work to produce four ZnS−Au samples with increasing densities of satellite Au (denoted as ZnS−Au-1, ZnS−Au-2, ZnS−Au-3, and ZnS−Au-4, respectively).

Preparation of ZnS@Au Counterpart. ZnS@Au counterpart was prepared by mixing pure ZnS nanospheres with Au colloids (with the concentration of 180 μM), which resulted in a random distribution of Au nanoparticles around ZnS nanospheres.

Preparation of Au-Loaded P-25 TiO_2. Au-loaded P-25 TiO_2 (denoted as TiO_2@Au) was prepared by mixing Degussa P-25 TiO_2 powder with Au colloids (with the concentration of 180 μM). A random distribution of Au around TiO_2 nanoparticles also resulted.

Photocatalytic Performance Measurement. The photocatalytic performance of ZnS−Au nanoassemblies was evaluated by the photodegradation of thionine (denoted as TH) under UV illumination. A quartz tube with a capacity of 15 mL was used as the photoreactor vessel. The optical system used for photocatalytic reaction was consisted of a xenon lamp (500 W) with a light

(18) (a) Zheng, Y.; Zheng, L.; Zhan, Y.; Lin, X.; Zheng, Q.; Wei, K. *Inorg. Chem.* **2007**, *46*, 6980. (b) Elmalem, E.; Saunders, A. E.; Costi, R.; Salant, A.; Banin, U. *Adv. Mater.* **2008**, *20*, 4312. (c) Costi, R.; Saunders, A. E.; Elmalem, E.; Salant, A.; Banin, U. *Nano Lett.* **2008**, *8*, 637. (d) Formo, E.; Lee, E.; Campbell, D.; Xia, Y. *Nano Lett.* **2008**, *8*, 668. (e) Chen, H.; Chen, S.; Quan, X.; Yu, H.; Zhao, H.; Zhang, Y. *J. Phys. Chem. C* **2008**, *112*, 9285. (f) Cheng, W.-Y.; Chen, W.-T.; Hsu, Y.-J.; Lu, S.-Y. *J. Phys. Chem. C* **2009**, *113*, 17342.

(19) (a) Zeng, H.; Cai, W.; Liu, P.; Xu, X.; Zhou, H.; Klingshirn, C.; Kalt, H. *ACS Nano* **2008**, *2*, 1661. (b) Zeng, H.; Liu, P.; Cai, W.; Yang, S.; Xu, X. *J. Phys. Chem. C* **2008**, *112*, 19620. (c) Li, J.; Xu, J.; Dai, W.-L.; Fan, K. *J. Phys. Chem. C* **2009**, *113*, 8343.

(20) Reber, J.-F.; Meier, K. *J. Phys. Chem.* **1984**, *88*, 5903.

(21) (a) Turkevich, J.; Hillier, J.; Stevenson, P. C. *Discuss. Faraday Soc.* **1951**, *11*, 55. (b) Ji, X.; Song, X.; Li, J.; Bai, Y.; Yang, W.; Peng, X. *J. Am. Chem. Soc.* **2007**, *129*, 13939.

intensity of 175 mW/cm^2. All the photocatalysis experiments were conducted at room temperature. Four kinds of photocatalysts including Au-loaded P-25 TiO_2, commercial ZnS powders (Sigma-Aldrich, with the particle size of 100−200 nm), ZnS@Au counterpart, and ZnS−Au nanoassemblies were used and compared in the photodegradation of TH. In a typical experiment, 3.0 mg of photocatalyst was added into 15 mL of TH solution in the photoreactor vessel. The TH solution was prepared by dissolving thionine acetate ($C_{14}H_{13}N_3O_2S$) in deaerated ethanol with a concentration of 2.5×10^{-5} M. Note that ethanol was used as the sacrificial hole scavenger for photocatalyst to facilitate the further utilization of photoexcited electrons. Prior to irradiation, the suspension was stirred in the dark for 30 min to reach the adsorption equilibrium of TH with photocatalyst. At certain time intervals of irradiation, 1.5 mL of the reaction solution was withdrawn and centrifuged to remove the photocatalyst particles. The filtrates were analyzed with a UV−vis spectrophotometer to measure the concentration variation of TH through recording the corresponding absorbance of the characteristic peak at 605 nm. To investigate the reusability and stability of photocatalyst, three cycles of photocatalytic reactions were conducted by using nanoassemblies of ZnS−Au-3 as the representative sample.

Characterizations. The morphology and dimensions of the products were examined with a transmission electron microscope (TEM, JEOL, JEM-2100) operated at 200 kV. The crystallographic structures of the samples were investigated with a X-ray diffractometer (XRD, MAC Sience, MXP18) and high-resolution TEM (HRTEM, JEOL, JEM-3000) operated at 300 kV. The compositional information was obtained with an energy dispersive spectrometer (EDS), an accessory of the HRTEM (JEM-3000), and X-ray photoelectron spectroscope (XPS, VG Scientific, Microlab 350). XPS measurement was performed using Mg Kα ($h\nu$ = 1253.6 eV) as X-ray source under a base pressure of 1.0×10^{-9} Torr. Samples were prepared by dripping the solution of a sufficient amount onto Si wafers (0.5 cm × 0.5 cm), followed by a heat treatment at 70 °C for 20 min to remove the solvent. The spectrum resolution was 0.1 eV, and the pass energy for survey and fine scans of core levels was 40 eV. All the binding energies were calibrated by C 1s at 284.6 eV. In this work, N 1s and C 1s XPS spectra of samples were fitted using XPSPEAK software. The deconvolution peaks, corrected by a linear baseline, were 15% Lorentzian and 85% Gaussian with the full widths at half-maximum (fwhm) ranging from 1.3 to 3.3 eV. The fwhm values of all the deconvolution peaks are basically in agreement with those reported in the literature. UV−vis absorption spectra were recorded using a Hitachi U-3900H. For photoluminescence spectroscopy, a Hitachi F-4500 equipped with a xenon lamp (150 W) was used. The excitation wavelength was set at 300 nm.

Results and Discussion

First, Au nanoparticles with an average diameter of 15 nm were obtained with the citrate reduction method.[21] A coupling event between Au nanoparticles and Cys/Zn complexes was then conducted through the direct mixing of them. The subsequent hydrothermal treatment at 130 °C for 6 h resulted in a purple-gray suspension. TEM observations revealed that the product consisted of a large quantity of nanospheres surrounded by a few tiny particles, as shown in Figure 1. These nanospheres were with a typical diameter of 180−230 nm, while the size of tiny particles was about 15 nm. Interestingly, as increasing the concentration of Au added, there is increasing density of tiny particles that encircled each nanosphere in the resulting products. In addition, a slight increase in size and partial aggregation among particles were observed for those tiny particles when Au colloids with higher concentrations (180 and 225 μM) were employed. On the basis of the above survey as well as the evident TEM contrast between nanospheres and tiny particles, we supposed that

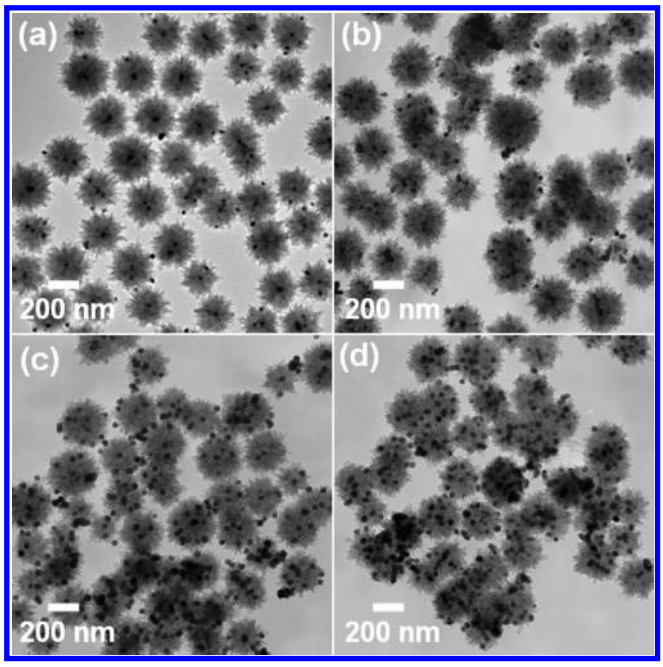

Figure 1. TEM images of ZnS−Au nanoassemblies with the Au concentrations of (a) 45, (b) 90, (c) 180, and (d) 225 μM.

nanospheres were composed of ZnS, while the tiny particles were the first-added Au. Such core−satellite architecture of ZnS−Au in the products can be further confirmed with the corresponding XPS, XRD, and HRTEM analyses.

The compositions and chemical states of the as-synthesized products were analyzed with XPS. In Figure 2a, both of the Zn and S XPS spectra exhibit signals consistent with the presence of ZnS with the binding energies of 1022.1 and 162.3 eV for Zn $2p_{3/2}$ and S 2p core levels, respectively.[22] This result implies the formation of ZnS upon the hydrothermal reaction. For the S 2p spectrum of products, note that no sulfate-related peak, which is located at around 168.4 eV,[23] was observed. It is well-known that sulfides such as CdS and ZnS easily undergo serious photocorrosive oxidation in the presence of oxygen and water. Such photocorrosion usually results in the production of sulfate ions.[20,24] The absence of sulfate-related peak in S 2p spectrum indicates that the as-synthesized ZnS-based products did not suffer significant photocorrosive oxidation and exhibited considerably high stability in air, which is important to the durability performance during their use as photocatalysts. XRD patterns of Figure 2b reveal the existence of wurtzite ZnS along with fcc Au in the products. To further ascertain the compositions within each nanoassembly, we performed TEM-EDS measurements. The TEM-EDS elemental mapping of Au, Zn, and S shown in Figure 3a confirms the core−satellite feature of ZnS−Au nanoassemblies. Figure 3b,c further shows the detailed crystallographic structures of the as-obtained ZnS−Au nanoassemblies. In Figure 3b, an HRTEM image taken at the interface of core and satellite regions of a single assembly, two distinct sets of lattice fringes were revealed. An interlayer spacing of 0.33 nm was observed in the core nanosphere, in good agreement with the d spacing of the (100) lattice planes of the wurtzite ZnS crystal.[25] For the satellite particle, an interlayer spacing of 0.24 nm was

(22) (a) Chen, S.; Liu, W. *Langmuir* **1999**, *15*, 8100. (b) Öznülüer, T.; Erdoğan, İ.; Demir, U. *Langmuir* **2006**, *22*, 4415.
(23) Antoun, T.; Brayner, R.; Al terary, S.; Fiévet, F.; Chehimi, M.; Yassar, A. *Eur. J. Inorg. Chem.* **2007**, 1275.
(24) Meissner, D.; Memming, R.; Kastening, B. *J. Phys. Chem.* **1988**, *92*, 3476.
(25) For bulk wurtzite ZnS, d(100) = 0.3309 nm from JCPDS 05-0492.

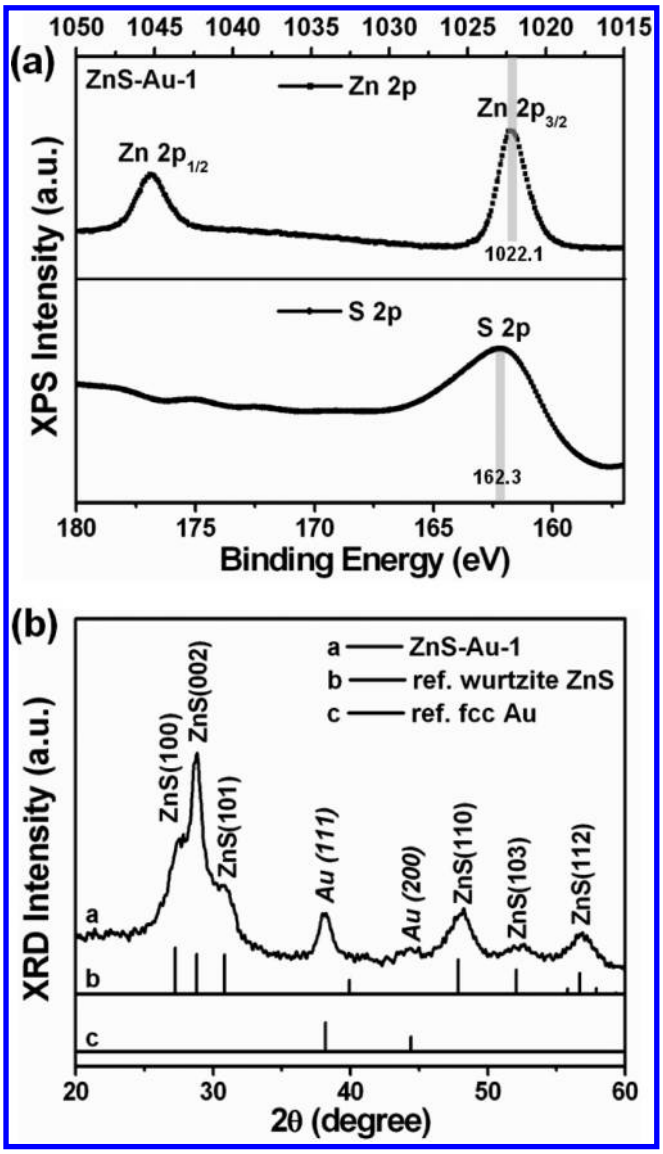

Figure 2. (a) Zn 2p and S 2p XPS spectra and (b) XRD pattern recorded for ZnS−Au nanoassemblies. In (b), the patterns of reference wurtzite ZnS (JCPDS 05-0492) and fcc Au (JCPDS 04-0784) were also included for comparison. Concentration of Au = 45 μM.

obtained, complying with the lattice spacing of the (111) planes of the fcc Au.[26] The corresponding electron diffraction pattern in Figure 3c further verifies the presence of both ZnS and Au nanocrystals with two sets of diffraction patterns indexed as wurtzite ZnS and fcc Au, respectively. This result, together with those of XPS, XRD, HRTEM, and TEM-EDS analyses, confirms the formation of core−satallite ZnS−Au nanoassemblies by using (Cys/Zn)−Au as the starting material in the hydrothermal reaction.

The success of this work to fabricate core−satellite nanoassemblies relied on the utilization of Cys as the trifunctional reagent in the hydrothermal process. With three functional groups (SH, COOH, NH_2), Cys was typically used as the sulfur source and reaction stabilizer for the growth of sulfide nanocrystals.[27] In the current synthetic system, Cys provided thiol groups forming fairly stable Cys/Zn complexes with Zn^{2+} ions,[28] amine groups binding Au to Cys/Zn complexes,[29] and carboxyl groups stabilizing the core ZnS. A plausible mechanism for the formation of ZnS−Au nanoassemblies is proposed as follows. At the beginning of synthesis, Au nanoparticles coupled with Cys/Zn complexes through the linkage between Au atoms and amine groups of Cys. Note that both thiol and amine groups of Cys exhibit binding abilities toward Au particles.[30] In the current synthetic system, since the thiol groups of Cys were predominately bonded to Zn^{2+} to form Cys/Zn complexes, the available sites of Cys allowed for further coupling with Au would mainly be amine groups. On the other hand, the pH value of Cys/Zn solution was around 3.5. Under this acidic regime, the amine groups of Cys were certainly capable of binding with Au particles.[31] The coupling event between Au and Cys/Zn can be further confirmed by the formation of nitride constituent (Au−N bonds) observed in the corresponding XPS analysis of Figure 4a. In Figure 4a, the deconvolution of N 1s peak produced three chemical states: the N1 component at 398.5 eV, which was assigned to a nitride constituent (Au−N), the N2 component at 399.6 eV, resulting from the amine groups (C−N) of Cys, and the N3 component at 401.2 eV, corresponding to the protonated amine (NH_3^+) of Cys.[32] Upon the hydrothermal reaction at 130 °C for 6 h, Cys/Zn complexes decomposed to yield ZnS nanospheres, while the initially bound Au nanoparticles remained at the surfaces of ZnS, producing the architecture of core−satellite ZnS−Au. It should be noted that Au-free ZnS nanospheres or free-standing Au particles were rarely observed in the products, demonstrating the advantage of the current synthetic approach to obtain core−satellite nanoassemblies. Additionally, the as-synthesized core−satellite nanoassemblies of ZnS−Au retained high dispersity in water, attributable to the remaining carboxyl groups of Cys at their surfaces. As shown in Figure 4b, the C 1s XPS peak at 288.9 eV (C2 component) reveals the existence of carboxyl groups[33] at the surfaces of nanoassemblies. The good dispersion for nanoassemblies may facilitate their future processing in wet media, which is crucial to the performance of practical use. As a final note, the substantial interface of ZnS/Au that formed in ZnS−Au nanoassemblies (highlighted by the dashed line in Figure 3b) may ensure the successful transfer of photoexcited electrons from ZnS to Au upon light irradiation and thus the achievement of charge separation.

We previously reported that core−shell Au−CdS nanocrystals can be obtained with a hydrothermal approach similar to the present one.[34] The difference in the growth habits between CdS and ZnS during the hydrothermal process may account for the structural divergence observed correspondingly. For core−shell Au−CdS nanocrystals case, it was believed that the first added Au nanoparticles acted as the seeds for the later growth of CdS. With the coupling between Au and Cys/Cd, CdS could nucleate

(26) For bulk fcc Au, d(111) = 0.2355 nm from JCPDS 04-0784.

(27) (a) Tong, H.; Zhu, Y.-J.; Yang, L.-X.; Li, L.; Zhang, L.; Chang, J.; An, L.-Q.; Wang, S.-W. *J. Phys. Chem. C* **2007**, *111*, 3893. (b) Xiong, S.; Xi, B.; Xu, D.; Wang, C.; Feng, X.; Zhou, H.; Qian, Y. *J. Phys. Chem. C* **2007**, *111*, 16761. (c) Xiang, J.; Cao, H.; Wu, Q.; Zhang, S.; Zhang, X.; Watt, A. A. R. *J. Phys. Chem. C* **2008**, *112*, 3580.

(28) (a) Bae, W.; Mehra, R. K. *J. Inorg. Biochem.* **1998**, *70*, 125. (b) Chatterjee, A.; Priyam, A.; Bhattacharya, S. C.; Saha, A. *Colloids Surf., A* **2007**, *297*, 258. (c) Rebilly, J.-N.; Gardner, P. W.; Darling, G. R.; Bacsa, J.; Rosseinsky, M. J. *Inorg. Chem.* **2008**, *47*, 9390.

(29) (a) Yang, Y.; Shi, J.; Chen, H.; Dai, S.; Liu, Y. *Chem. Phys. Lett.* **2003**, *370*, 1. (b) Sheeney-Haj-Ichia, L.; Pogorelova, S.; Gofer, Y.; Willner, I. *Adv. Funct. Mater.* **2004**, *14*, 416.

(30) Zhong, Z.; Subramanian, A. S.; Highfield, J.; Carpenter, K.; Gedanken, A. *Chem.—Eur. J.* **2005**, *11*, 1473.

(31) Zhong, Z.; Patskovskyy, S.; Bouvrette, P.; Luong, J. H. T.; Gedanken, A. *J. Phys. Chem. B* **2004**, *108*, 4046.

(32) Adenier, A.; Chehimi, M. M.; Gallardo, I.; Pinson, J.; Vila, N. *Langmuir* **2004**, *20*, 8243.

(33) Ramanathan, T.; Fisher, F. T.; Ruoff, R. S.; Brinson, L. C. *Chem. Mater.* **2005**, *17*, 1290.

(34) Chen, W.-T.; Yang, T.-T.; Hsu, Y.-J. *Chem. Mater.* **2008**, *20*, 7204.

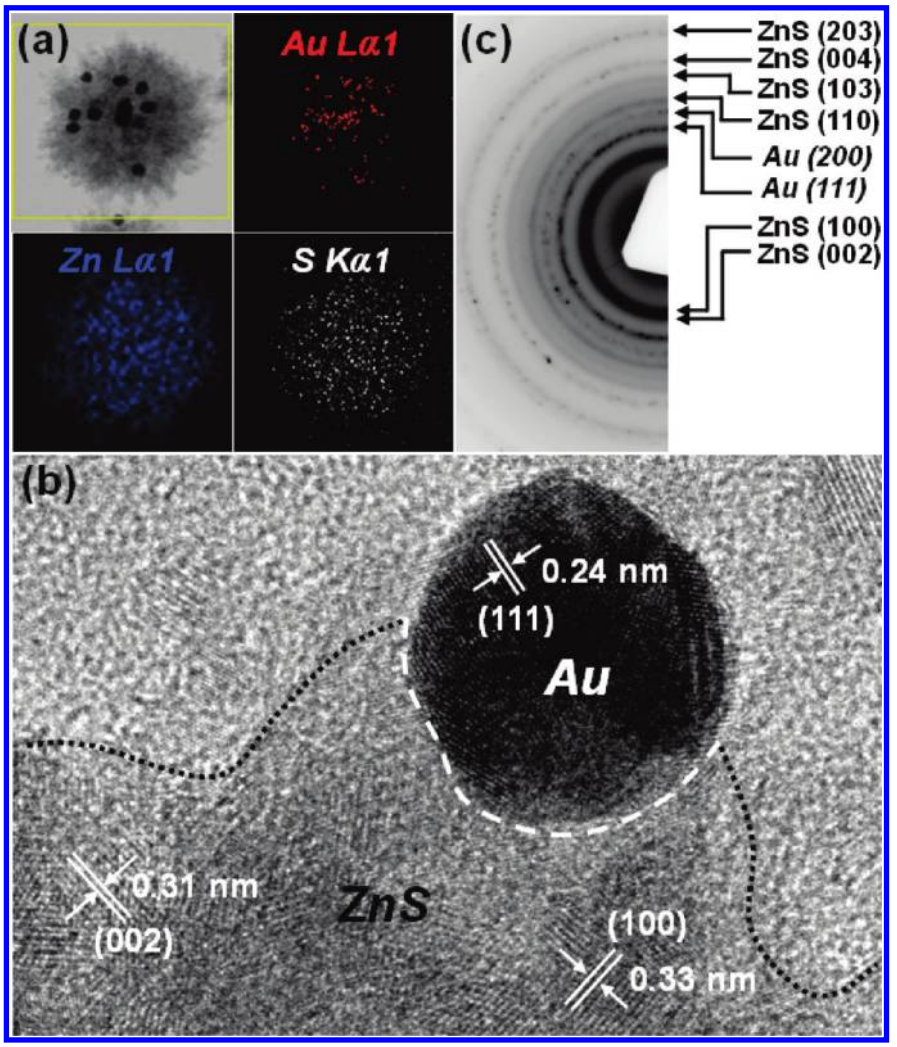

Figure 3. (a) TEM-EDS elemental mapping, (b) HRTEM image, and (c) the corresponding SAED pattern taken on a single ZnS−Au nanoassembly. In (b), the boundary of ZnS nanosphere and the interface of ZnS/Au were highlighted with the dotted and dashed lines, respectively. Concentration of Au = 45 μM.

heterogeneously and grow more readily at the surfaces of Au, resulting in the formation of core−shell structures. As for the case of ZnS−Au nanoassemblies, Au nanoparticles instead were less involved in the growth of ZnS. The coupling between Au and Cys/Zn was more significant and accountable to the direct contact of Au with ZnS that existed in the resulting ZnS−Au nanoassemblies. The above argument can be validated by the fact that without the addition of Au, ZnS itself can grow as nanospheres as it did in ZnS−Au case. This phenomenon implies the prevalence of homogeneous nucleation of ZnS in the hydrothermal growth of ZnS−Au nanoassemblies. In fact, the concentration of Cys/Zn (50 mM) employed here is substantially higher than that of Cys/Cd (5 mM) used in the Au−CdS system. When a reduced Cys/Zn concentration is applied, the resultant relatively low supersaturation may alter the growth habit of ZnS, enabling ZnS to nucleate heterogeneously and grow at the surfaces of Au. Under this circumstance, core−shell Au−ZnS nanocrystals may result.[34]

The optical properties of ZnS−Au nanoassemblies prepared with four various Au concentrations were characterized with UV−vis and photoluminescence (PL) spectroscopy. For comparison purposes, pure ZnS nanospheres were also prepared and analyzed here. As displayed in Figure 5a, all the ZnS-based samples showed an absorption edge at around 330 nm, consistent with the bulk bandgap energy of ZnS (E_g = 3.7 eV). Moreover, an additional absorption band at about 570 nm was observed for ZnS−Au with higher Au concentrations (ZnS−Au-3 and ZnS−Au-4). This band can be attributed to the typical surface plasmon resonance (SPR)[35] absorption that originated from the satellite Au in nanoassemblies. In addition to the emergence of SPR absorption, the color change of ZnS upon the introduction of Au was also evident. As illustrated in the inset of Figure 5a, the color of ZnS−Au solutions turned purple with increasing Au concentration, which is also characteristic of the SPR of Au. The present core−satellite ZnS−Au nanoassemblies provide an ideal platform to investigate the photoinduced charge transfer property for the ZnS/Au hybrid system. Note that the satellite Au can serve as an effective electron scavenger for the core ZnS. The conduction band of ZnS is located at around −1.85 V vs NHE,[20] higher in the energetic state than the Fermi level of Au (+0.5 V vs NHE).[17a] Consequently, the photoexcited free electrons in core ZnS would preferentially transfer to satellite Au, leading to the depletion of free electrons in ZnS domain and the subsequent suppression of excitonic emission of ZnS. Figure 5b shows the PL spectra of the as-synthesized ZnS−Au nanoassemblies compared with that of pure ZnS nanospheres. A rather broad emission

(35) (a) Mulvaney, P. *Langmuir* **1996**, *12*, 788. (b) Eustis, S.; El-Sayed, M. A. *Chem. Soc. Rev.* **2006**, *35*, 209.

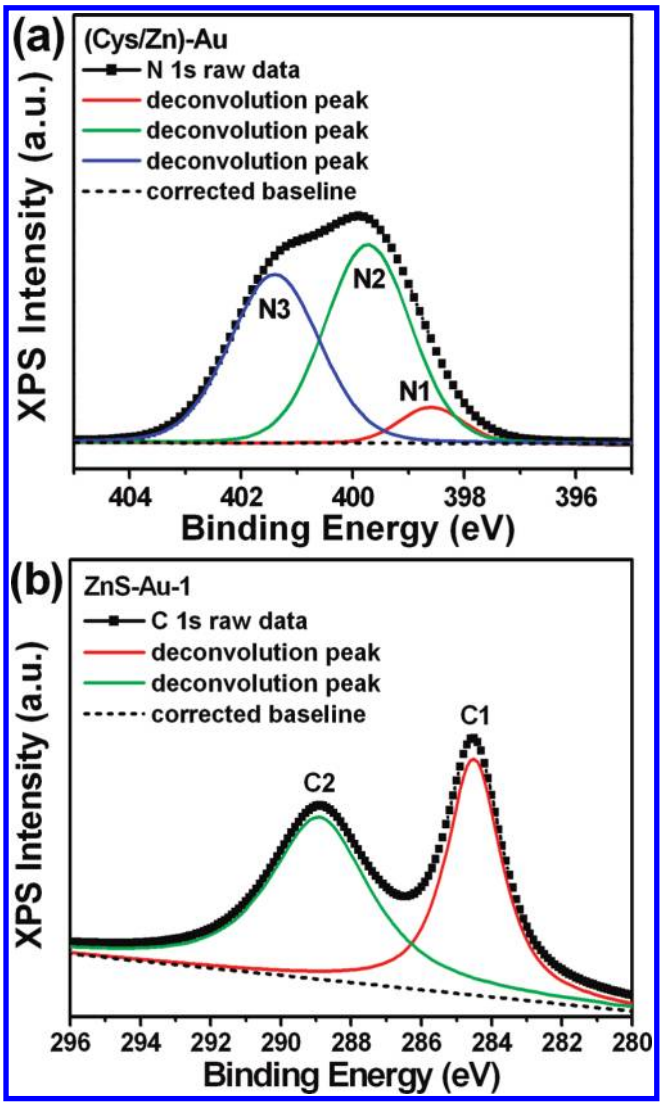

Figure 4. (a) XPS spectrum of N 1s peak for Au-coupled Cys/Zn complexes. (b) XPS spectrum of C 1s peak for ZnS−Au nanoassemblies. Concentration of Au = 45 μM.

band, ranging from 330 to 480 nm, was observed for all the ZnS-based samples. Peak deconvolution revealed four primary emissions centered at 350, 380, 420, and 454 nm. The emission at 350 nm was attributed to the typical excitonic band-to-band radiative emission of ZnS due to its location near the absorption edge. The other three peaks were however assigned to the trap-state emissions, presumably coming from the various point defects present in ZnS.[36] More importantly, a significant quenching in the PL emission was observed for ZnS−Au nanoassemblies as compared to pure ZnS nanospheres. Such quenching became more noticeable as the concentration of Au was increased, implying the successful electron transfer from core ZnS to satellite Au. This demonstration supports our argument that Au acts as an effective electron scavenger for ZnS, leading to the pronounced photo-induced charge separation observed for ZnS−Au nanoassemblies.

To investigate the potential as a photocatalyst for the current ZnS−Au nanoassemblies, we performed a series of photocatalysis

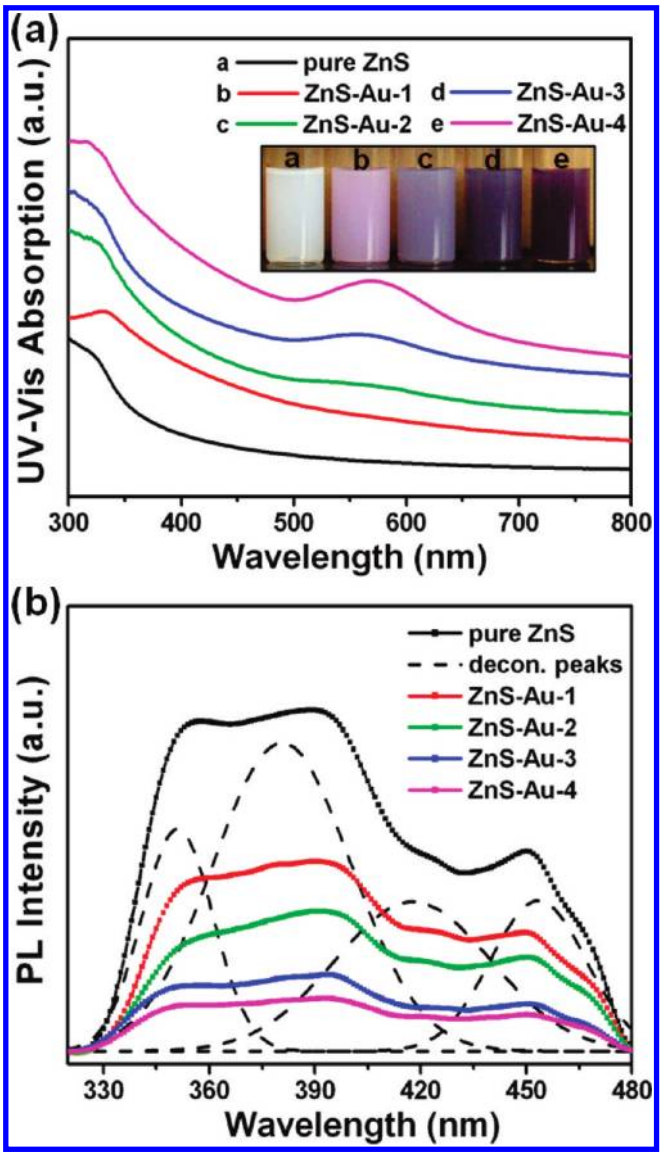

Figure 5. (a) UV−vis absorption and (b) PL emission spectra for pure ZnS nanospheres and ZnS−Au nanoassemblies with various Au concentrations. Inset in (a) shows the corresponding solution colors.

experiments. A cationic dye (TH), which is capable of accepting electrons following the UV irradiation on ZnS−Au nanoassemblies, was utilized as the indicator. The time-dependent absorption spectra of TH solutions under UV illumination in the presence of nanoassembly sample (ZnS−Au-1) were first shown in Figure 6a. It can be seen that the intensity of the characteristic peak at 605 nm decreased dramatically with the irradiation time. The bleaching of the absorption at 605 nm implies the reduction of TH to its leuco form,[37] verifying the successful transfer of photoexcited electrons from ZnS−Au to TH. To quantitatively understand the photodegradation of TH in the nanoassemblies, we analyzed the normalized concentration of TH (C/C_0) as a function of irradiation time. Figure 6b compares the photocatalytic performance among all the ZnS-based samples. Experiment in the absence of photocatalyst showed slight degradation of TH, indicating a minor extent of self-photolysis for TH molecules under UV illumination. For pure ZnS nanospheres, about 72% of TH was degraded after 75 min of irradiation. A higher extent of

(36) (a) Jiang, Y.; Meng, X.-M.; Liu, J.; Hong, Z.-R.; Lee, C.-S.; Lee, S.-T. *Adv. Mater.* **2003**, *15*, 1195. (b) Hu, P.; Liu, Y.; Fu, L.; Cao, L.; Zhu, D. *J. Phys. Chem. B* **2004**, *108*, 936. (c) Shen, X.-P.; Han, M.; Hong, J.-M.; Xue, Z.; Xu, Z. *Chem. Vap. Deposition* **2005**, *11*, 250. (d) Murugadoss, A.; Chattopadhyay, A. *Bull. Mater. Sci.* **2008**, *31*, 533.

(37) Hirakawa, T.; Kamat, P. V. *Langmuir* **2004**, *20*, 5645.

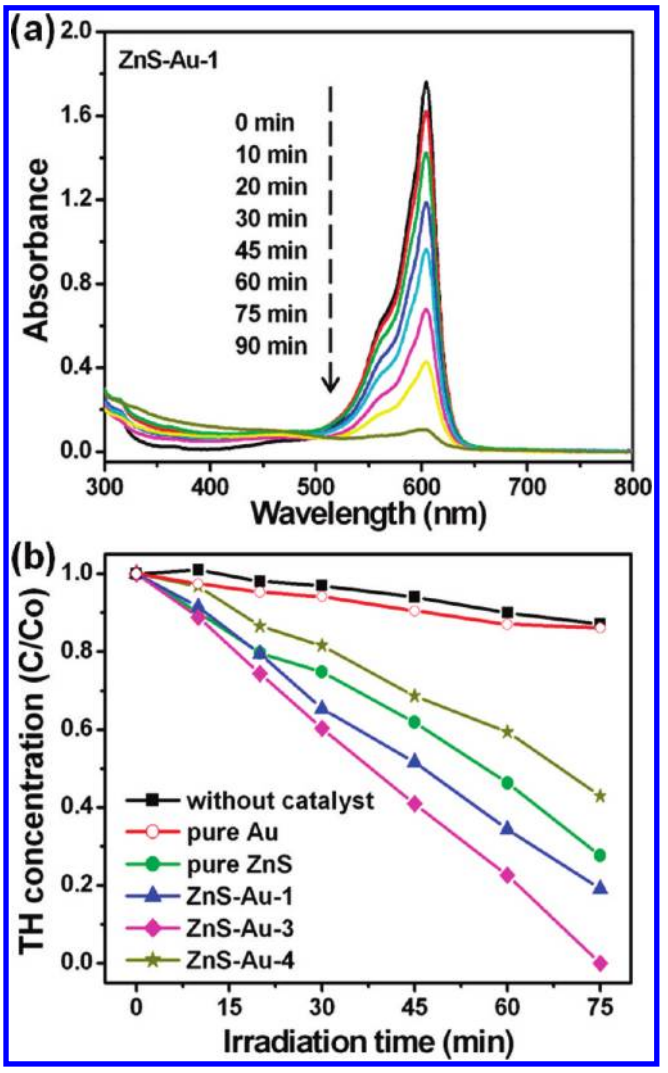

Figure 6. (a) Absorption spectra of TH solutions undergoing photodegradation in the presence of ZnS−Au nanoassemblies with different irradiation times. Concentration of Au = 45 μM. (b) C/C_0 vs irradiation time plots for TH photodegradation without any catalyst and in the presence of ZnS−Au nanoassemblies with various Au concentrations. The results by using Au nanoparticles (180 μM) and pure ZnS nanospheres were also included for comparison.

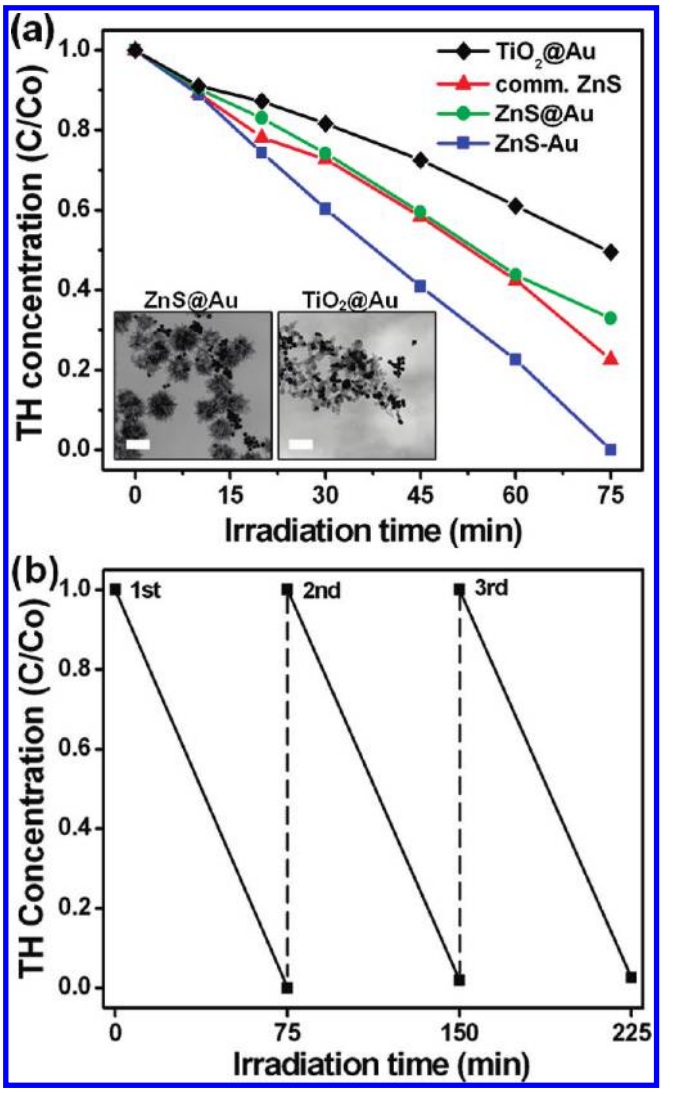

Figure 7. (a) C/C_0 vs irradiation time plots for TH photodegradation in the presence of different photocatalysts. (b) Recycling test on ZnS−Au nanoassemblies for TH photodegradation. Insets in (a) show the TEM images of ZnS@Au counterpart and TiO_2@Au, and the scale bar is 250 nm. Concentration of Au = 180 μM.

TH photodegradation to around 81% at the same irradiation time was achieved when using nanoassemblies of ZnS−Au-1. This is mainly a result of the satellite Au that can facilitate charge separation by attracting the photoexcited electrons of ZnS, thus providing more electrons for the reduction of TH. For ZnS−Au with higher Au concentration (ZnS−Au-3), an even better performance in TH photodegradation can be attained, presumably due to the much more conspicuous charge separation caused by the increasing amount of Au. Further increase in the concentration of Au for nanoassemblies (ZnS−Au-4) however led to a depressed efficiency of TH photodegradation. The excess content of Au may cover a large part of ZnS surfaces, which in turn decreases the number of active sites for photocatalysis. The high coverage of Au may also retard the access of UV irradiation to ZnS surfaces, resulting in a reduced amount of photoexcited charge carriers to decline the photocatalytic performance.[38] Moreover, as increasing the concentration of Au added, ZnS nanospheres were surrounded by more and more Au nanoparticles which tended to aggregate, as observed in Figure 1. These aggregated Au nanoparticles are more likely to play a role of electron−hole recombination center instead the electron trapper,[39] leading to a significant depletion of photoexcited charge carriers and thus the depression of photocatalytic efficiency. Since nanosized Au is catalytic to many chemical reactions, a concern about the possible contribution of Au toward TH photodegradation arises. To address this issue, we performed a control experiment by using Au nanoparticles as the catalyst for TH photodegradation. As shown in Figure 6b, a slight extent of TH degradation, which was mainly attributed to the self-photolysis effect of TH, was observed for Au nanoparticles. This outcome indicates that no significant contribution toward TH photodegradation was made by Au nanoparticles in the current system. This demonstration can further emphasize the beneficial effect of ZnS/Au interface on the photocatalytic performance of ZnS−Au nanoassemblies.

(38) Arabatzis, I. M.; Stergiopoulos, T.; Andreeva, D.; Kitova, S.; Neophytides, S. G.; Falaras, P. *J. Catal.* **2003**, *220*, 127.

(39) (a) Sclafani, A.; Herrmann, J. M. *J. Photochem. Photobiol. A* **1998**, *113*, 181. (b) Tahiri, H.; Ichou, Y. A.; Herrmann, J. M. *J. Photochem. Photobiol. A* **1998**, *114*, 219. (c) Lu, W.; Gao, S.; Wang, J. *J. Phys. Chem. C* **2008**, *112*, 16792.

To demonstrate the remarkable photocatalytic efficiency for ZnS−Au nanoassemblies, further comparative experiments were conducted. Four kinds of photocatalysts including Au-loaded P-25 TiO_2 (TiO_2@Au), commercial ZnS powders, ZnS@Au counterpart, and core−satellite ZnS−Au nanoassemblies were used for TH photodegradation under the same experimental conditions. Note that ZnS@Au counterpart was prepared by simply mixing pure ZnS nanospheres with Au colloids, resulting in a random distribution of Au nanoparticles around ZnS nanospheres. The comparative results are shown in Figure 7a, from which several points can be observed. First, as compared to the relevant commercial products like TiO_2@Au and ZnS powders, ZnS−Au nanoassemblies exhibited superior photocatalytic performance, demonstrating their potential as an efficient photocatalyst in relevant redox reactions. Second, ZnS−Au nanoassemblies performed better toward TH photodegradation than ZnS@Au counterpart did, which can be accounted for by the effective contact of Au with ZnS that existed in ZnS−Au. As shown in Figure 3b, a direct contact of Au with ZnS to form the substantial ZnS/Au interface was observed in ZnS−Au, with which the transfer of photoexcited electrons from ZnS to Au can proceed to achieve charge carrier separation. As regards the ZnS@Au counterpart, very less contact of Au with ZnS was existent, as can been clearly seen from the TEM image shown in the inset of Figure 7a. The limited contact of Au with ZnS in ZnS@Au may further retard the occurrence of charge carrier separation, leading to a poor photocatalytic performance as observed. This result reaffirms the effective charge separation that occurred in ZnS−Au nanoassemblies and its benefit to the photocatalytic performance. This demonstration also addresses the uniqueness of the current synthetic route, through which core−satellite nanoassemblies of ZnS−Au with remarkable photocatalytic efficiency can be obtained. To evaluate the reusability and stability of ZnS−Au nanoassemblies, we further performed a recycling test by using ZnS−Au-3 as the representative photocatalyst. As shown in Figure 7b, no appreciable decay of photocatalytic activity was found for ZnS−Au nanoassemblies after they were repeatedly used and recycled in TH photodegradation for three times. This result reveals that the current core−satellite nanoassemblies could be promisingly utilized in the long-term course of photocatalysis.

Conclusions

In conclusion, we have developed a facile L-cysteine-assisted hydrothermal approach for preparing core−satellite ZnS−Au nanoassemblies. The growth of ZnS−Au nanoassemblies involved the binding of Au nanoparticles toward Cys/Zn complexes, followed by the hydrothermal decomposition of Cys/Zn and the subsequent growth of ZnS nanospheres that were surrounded by Au nanoparticles. By suitably modulating the concentration of Au added, a controllable density of Au nanoparticles that encircled each ZnS nanosphere can be achieved. Because of the band offsets between ZnS and Au, a pronounced photoinduced charge separation was observed for the as-synthesized ZnS−Au nanoassemblies. As compared to the relevant commercial products like Au-loaded P-25 TiO_2 and ZnS powders, ZnS−Au nanoassemblies exhibited superior photocatalytic performance toward TH photodegradation, attributable to the effective charge separation that took place at the interface of ZnS/Au. The current ZnS−Au nanoassemblies may find potential applications in relevant photocatalytic reactions such as water splitting and organics degradation. Moreover, ZnS−Au nanoassemblies retained comparable photocatalytic activity after repeated uses and recycled, revealing that ZnS−Au could be promisingly utilized in the long-term course of photocatalysis. The present study provides a new paradigm for designing the highly efficient semiconductor/metal hybrid photocatalysts that can effectively produce chemical energy from light.

Acknowledgment. This work was financially supported by the National Science Council of the Republic of China (Taiwan) under Grants NSC-97-2221-E-009-073 and NSC-98-2218-E-009-003.